



ELSEVIER

Available online at www.sciencedirect.com

SCIENCE @ DIRECT®

Electronic Notes in Discrete Mathematics 20 (2005) 475–491

Electronic Notes in
DISCRETE
MATHEMATICS

www.elsevier.com/locate/ndm

Reconstruction of pixel-based and geometric objects by discrete tomography. Simulation and physical experiments[★]

Zoltán Kiss^{a,1}, Lajos Rodek^{a,2}, Antal Nagy^{a,2},
Attila Kuba^{a,2}, and Márton Balaskó^{b,3}

^a *Dept. of Image Proc. and Computer Graphics, Univ. of Szeged, Szeged, Hungary*

^b *KFKI Atomic Energy Research Institute, Budapest, Hungary*

Abstract

Tomography is an imaging technique to reconstruct cross-sections of objects from projection images in a non-destructive way. We have implemented two discrete tomographic (DT) reconstruction methods. The first method is general in the sense that the objects to be reconstructed are represented by pixels, and in this way the method can be used for reconstructing any shape. The second one is able to reconstruct objects consisting of cylinders and spheres made of homogeneous materials only. Simulation and physical experiments connected with non-destructive testing by X-rays were performed, and the results are presented.

Keywords: discrete tomography, simulated annealing, optimization, stochastic relaxation

[★] This work was supported by the NSF grant DMS0306215 (Aspects of Discrete Tomography) and the OTKA grant T 048476 (New Aspects and Applications of Discrete Tomography in Neutron Radiography).

¹ Corresponding author. Email: kissz@inf.u-szeged.hu

² Email: {rodek,nagya,kuba}@inf.u-szeged.hu

³ Email: balasko@sunserv.kfki.hu

1 Introduction

Many industrial applications need a procedure to get some information about the structure of the object to be investigated in a non-destructive manner. X-ray tomography is such a technique, performing reconstructions of cross-sections of the object from X-ray transmission projections. Nevertheless, the acquisition of such projection images is an expensive and time consuming procedure, so one of the main efforts is to minimize the number of projections used for the reconstruction. A possible approach to achieve this aim is the application of discrete tomographic (DT) methods. It means that a special class of objects can be reconstructed, when the object comprises only a few homogeneous materials that can be characterized by known absorption values. Accordingly, the result of a DT reconstruction is a *discrete image* having values only corresponding to the few known absorption coefficients. An overview of theory, algorithms, and applications of DT can be found in [3].

Discrete tomography is an image reconstruction technique, where the goal is to find an image function whose projections approximate the real, physically measured ones as closely as possible. A substantial difference between classic computed tomography (CT) and discrete tomography is that in DT the range of the image function consists of finitely many *known values*. Moreover, in many cases some *a priori information* is also available about the object under investigation, such that its structure is similar to that of a template object, or that the object is made of materials that are at least nearly homogeneous. An important application of discrete tomography is the industrial non-destructive testing (NDT) when the internal configuration of a specimen is to be determined without causing any damage.

This paper introduces an extension and experiments of two kinds of DT techniques, which can be applied to reconstruct even multi-level discrete images (i.e., their range contains more than two values) from their projections. Both algorithms consider the reconstruction problem as an optimization task discussed in Section 2. The difference between the algorithms is in the representation of the object under investigation. In both cases the reconstruction is solved by an optimization based on simulated annealing. For more details about the adaptation, see [5,6].

One of the reconstruction techniques is a pixel-based method that considers the object as a digital image. The main advantage of the pixel-based method is that it is general in the sense that it can be used for reconstructing any shape. This method is described in Subsection 2.1.

The other algorithm reconstructs objects consisting of circles, cylinders

and spheres made of homogeneous materials only. Such 2D and 3D geometric objects can be represented by a few parameters like radii, positions, heights, etc. In this case the reconstruction determines the parameters of the geometric objects, in other words the optimization carries out a search in the space of parameters. This parameter-based method is presented in Subsection 2.2.

In order to assess the efficiency of these techniques, several simulation experiments were done. We were also interested in how certain reconstruction parameters (e.g. the number of projections) or the amount of noise affect the reconstructed image. These results and conclusions are shown in Section 3. We had the opportunity to test both algorithms also for reconstructing real, not necessarily binary objects. The results of these X-ray experiments are given in Section 4.

The physically measured projections are not suitable for immediate reconstruction due to several properties and defects of the image acquisition system (e.g., non-uniform sensitivity during acquisition time and on the detector plate, bright specks, presence of statistical noise, etc.). Hence, some pre-processing steps are necessary to reduce these effects. These correction steps are summarized in Subsection 4.3.

The algorithms presented here have been incorporated into the system called DIRECT [7], what is a framework, being developed for testing and visualizing various DT methods.

2 The pixel- and parameter-based methods for multi-level images

Non-destructive testing (NDT) is an industrial procedure, where several kinds of objects are imaged using some transmission rays, like X-rays or neutron rays. The rays transmitted through the object are then partially absorbed by the materials comprising the object. The relation between the initial (unabsorbed) and transmitted intensities, I_S and I_D respectively, can be expressed as a function that depends on the absorption coefficient (μ) of the object. That is

$$(1) \quad I_D(s, \vartheta) = I_S \cdot e^{-\int_s^D \mu(u) du} .$$

This equation is a basic relation in transmission *tomography*, where the cross-sections of the object being studied are to be determined from such measurements. Mathematically the transmission tomography is modelled by the *Radon transformation*, giving the line integrals of a two-dimensional integrable

function f , denoted by $\mathcal{R}f$. Formally,

$$(2) \quad [\mathcal{R}f](s, \vartheta) = \int_{-\infty}^{\infty} f(x, y) du ,$$

where s and u denote the variables of the coordinate system rotated by ϑ . The function $\mathcal{R}f$ for a fixed value of ϑ is also called the ϑ -angle *projection* of f .

Let f denote the absorption coefficients of the 2D object being studied. Then the ϑ -angle projection of f can be computed from the transmission measurements after a suitable *logarithmic transformation*. That is

$$(3) \quad [\mathcal{R}f](s, \vartheta) = \ln \frac{I_S}{I_D(s, \vartheta)} .$$

Now the *reconstruction problem* can be posed as to find a function f such that its projections are equal to some given functions. In other words, we are looking for the inverse of \mathcal{R} , i.e., $\mathcal{R}^{-1}g$. The function f is sometimes called the *image function*, or briefly the *image*.

Both methods to be presented consider the reconstruction as an optimization task that is solved by the adaptation of simulated annealing (SA), and that optimizes the following objective functional:

$$(4) \quad \Phi(f) = \sum_{\vartheta} \| [\mathcal{R}f](\vartheta) - P_{\vartheta} \|^2 ,$$

where P_{ϑ} denotes the acquired input projection of angle ϑ , f is the two-dimensional image function approximating the solution, and $[\mathcal{R}f](\vartheta)$ denotes the projection of the image f taken at angle ϑ . So, the aim is to find the image function f , whose corresponding projections are the most suitable for the input data.

2.1 The pixel-based method

The difference between the pixel- and the parameter-based techniques lies in the representation of the image function f . The *pixel-based* method represents the image function as a digital image, and it can reconstruct discrete functions in the following manner. Since SA is an iterative stochastic technique, at each iteration a new image function is produced in accordance with a (modification) *rule*, namely, the modification of the approximating image function created in the previous iteration step. In binary case (when the range of the image function is $\{0, 1\}$) the rule is to change the intensity of a randomly chosen pixel (from 1 to 0 or 0 to 1), where the position of that pixel

was generated randomly from a uniform distribution. For details of SA, its current adaptation, scheduling, binary studies, and experiments, see [2,4,5,6].

Since industrial objects are often made of more than 2 materials, it was desirable to enable the technique to reconstruct not only binary but multi-level images (cross-sections) as well. Since in this case the pixels can take their intensity values from $M = \{a_1, a_2, \dots, a_n\}$ (n is the number of possible intensity values), the obvious extension is a uniformly distributed random choice of an intensity level from M .

In order to improve the efficiency, we appended a regularization (penalty) term to (4) that held the a priori information about the image function to be reconstructed. So the new objective, which was used in the pixel-based method, is

$$(5) \quad \Phi(f) = \sum_{\vartheta} \|\mathcal{R}f(\vartheta) - P_{\vartheta}\|^2 + \gamma \cdot \phi(f) ,$$

where $\phi(f)$ is called the regularization term that embodies the a priori information, and $\gamma \geq 0$ is the so-called regularization parameter, which determines the weight between the two terms. A small γ prefers a result that is more suitable for the input projections, a large γ yields such an outcome, which is more appropriate for the a priori information. If the image to be reconstructed contains a few larger regions made of homogeneous materials, this information may be the *smoothness*, which can be, for example, the following functional:

$$(6) \quad \phi(f) = \sum_{x,y} \sum_{u,v} |f(x,y) - f(x-u,y-v)| \cdot e^{-\frac{1}{2} \left(\left(\frac{u}{\sigma_1} \right)^2 + \left(\frac{v}{\sigma_2} \right)^2 \right)} ,$$

where σ_1, σ_2 are suitable constants. In this study we set $\sigma_1 = \sigma_2$, their value depends on the image to be reconstructed.

2.2 The parameter-based method

Our second reconstruction method takes the assumption that the object is composed of a tube encompassing a solid cylinder called the interior (i.e. the inner space of the tube), which contains a known number of disjoint solid spheres or cylinders made of homogeneous materials. Furthermore, it is also assumed that at most four different homogeneous materials constitute the object, namely,

- the material of the tube,
- the material of the interior,
- the material of the spheres and cylinders, and

- the background surrounding the object, what is usually air or a vacuum.

Since spheres as well as cylinders can be described by a few parameters like center, height, and radius, each object can be represented as a vector of parameters called *configuration*. In order to perform a truly 3D reconstruction, the optimization of the objective functional $\Phi(f)$ is performed in the parameter space iteratively. Starting off from an initial configuration, the current configuration is altered at every iteration step to produce a better approximation of the object to be reconstructed. The modified configuration may be accepted only if it satisfies certain geometric restrictions. A more detailed description of the algorithm can be found in [5,6].

3 Simulation studies

3.1 Reconstruction of pixel-based objects

We reconstructed several multi-level phantom objects. One of the phantoms and one of its projections can be seen in Fig. 1(a) and (b). First, we performed reconstructions using the objective functional (4), but the technique did not give a satisfactory result, as shown in Fig. 1(c). The reason of the low quality might be the presence of the enhanced number of switching components (for the definition, see [3]) in case of multi-level images.

Since, especially in case of industrial objects, it may often be assumed that the image contains continuous regions of the same intensity, it was suspected that we would obtain better results having this criterion. Thus for the improvement we tried the reconstruction using (5), where the regularization term was the smoothness shown in (6). One of the results, we obtained this way by the usage of parallel beam arrangement, is shown in Fig. 1(d). It is seen that the method gave improved result by the assumption of smoothness, which gain could be exploited for the reconstruction of measured projections.

The pixel-based method is statistical, hence we calculated average images from results of 50 runs as well. Such average images are presented in Fig. 2. These images were generated from fan-beam projections in noiseless or noisy circumstances with or without smoothness. It can be observed that the method could reconstruct the original phantom image with small errors even in noisy case. However, some errors are seen especially along the edges of black and white regions, where the method substituted the sharp edge by a new region of a mediate intensity.

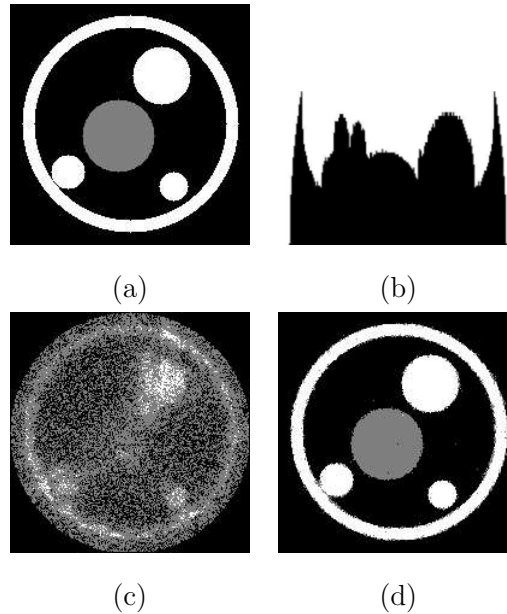


Fig. 1. (a) A 3-level phantom image used for simulation studies. (b) One of the projections of the object in (a). Reconstruction results from 12 noiseless projections, 400 measurements/projection (c) using the objective functional (4), and (d) using (5).

3.2 Reconstruction of parameter-based objects

The aim of the first simulation experiment was to examine the effects of geometric complexity of the object, using only 2 noisy projections. The complexity of the object was described by the number of spheres in the cylinder. As Fig. 3 shows, generally it is hard to produce an acceptable result if there are 5 or more spheres. The objects are modeled using the Virtual Reality Modeling Language (VRML97 [9]), and presented by the software system DIRECT [7].

It is also interesting how the amount of noise influences the result. This was studied in the second software experiment, as presented in Fig. 4 when 2 projections were used.

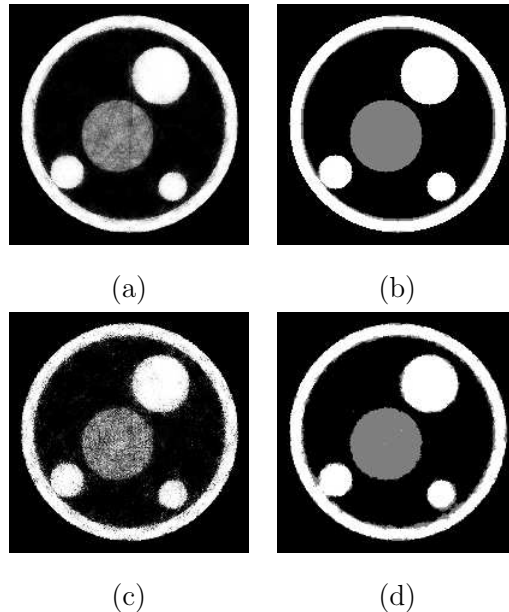


Fig. 2. Average of 50 reconstruction results (200×200) of the phantom in Fig. 1(a) using 16 fan-beam projections, 800 measurements/projection. (a) Average result from noiseless projections without using smoothness. (b) Average result from noiseless projections using smoothness in penalty term. (c) Average result from noisy (5% Gaussian) projections without using smoothness. (d) Average result from noisy (5% Gaussian) projections using smoothness in penalty term.

4 Experimental results

4.1 Test object

We had the opportunity to test our techniques using X-ray projection data. The phantom object was a so-called *reference cylinder*. It is a solid cylinder made of Plexiglas, containing three bores of different diameter and depth in an asymmetric arrangement (see Fig. 5(a)). The lower part of the deepest hole was filled with aluminum screws, as shown in Fig. 5(b).

4.2 Data acquisition

In order to image an object, several kinds of radiations (gamma, neutron, X, etc.) can be used. The principle of our apparatus of X-ray radiography presented here is widely used nowadays (see Fig. 6).

The object to be investigated is placed on a rotating table. The table can

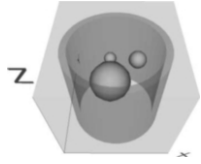
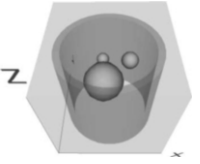
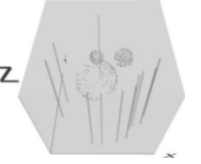
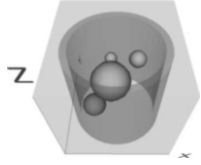
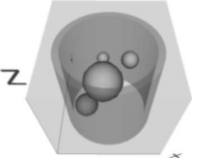
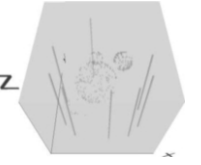
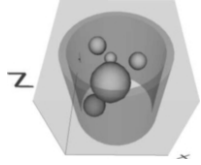
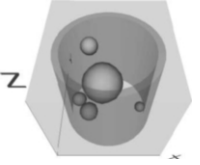
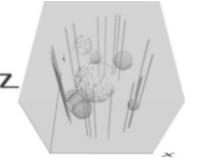
# of sph.	Original	Result	Difference
3			
4			
5			

Fig. 3. Reconstruction by parameter-based method using different number of spheres (parameters: 10% noise, 2 2-dimensional projections, 100×100 measurements/projection). First column: number of spheres. Second column: original object. Third column: reconstructed object. Fourth column: difference between the reconstructed and original object (only mismatching voxels are painted).

be rotated by a PC-controlled stepper motor, thus letting the beams transmit through the object in different directions. The beams attenuated by the object impact into a scintillator, which transforms the detected radiation into visible light detected by a CCD camera. Since the camera can be damaged by direct radiation, an optical mirror system conveys the light from the scintillator to the CCD camera. The images taken by the camera are stored temporarily by the camera controller, and finally a dedicated PC reads out the raw image data from this storage. A more thorough description of the imaging apparatus can be found in [1].

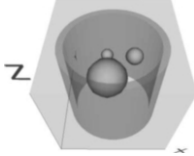
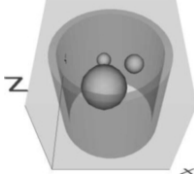
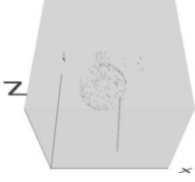
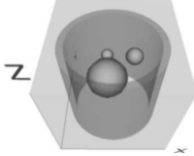
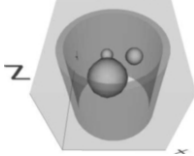
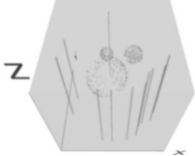
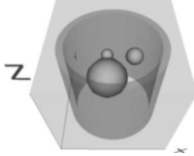
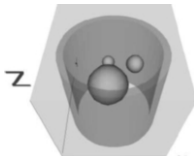
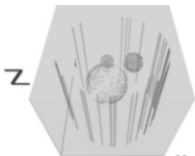
Noise (%)	Original	Result	Difference
0			
10			
40			

Fig. 4. Reconstruction by parameter-based method from noise-free and noisy projections (parameters: 3 spheres, 2 2-dimensional projections and 100×100 measurements/projection). First column: noise level. Second column: original object. Third column: reconstructed object. Fourth column: difference between the reconstructed and original object.

4.3 Pre-processing

Due to several distorting effects of the data acquisition system, the measured projections were not suitable for immediate reconstruction. These distortions were mostly caused by the physical properties of the imaging system. In order to diminish them some corrections, so-called *pre-processing steps* were performed on the projection data. In case of the reference cylinder these steps were the following:

- Since the reconstructions can be carried out only from line integrals of the absorption function, we transformed the original measured values into such integrals by the application of the logarithmic transformation given in (3).
- The total intensity of the projections varied projection to projection, which

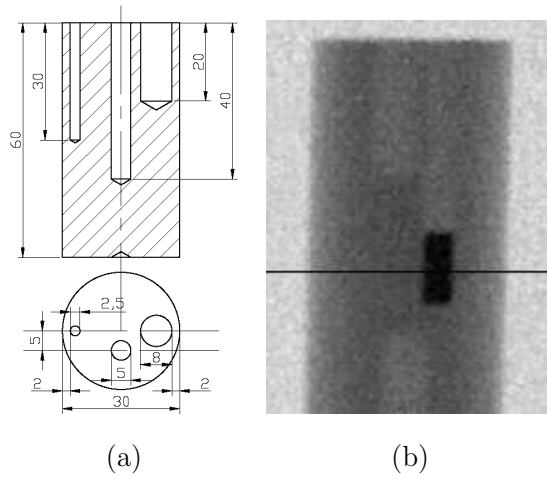


Fig. 5. (a) Diagram of the physical phantom object used in the X-ray experiments. (b) A projection image of (a).

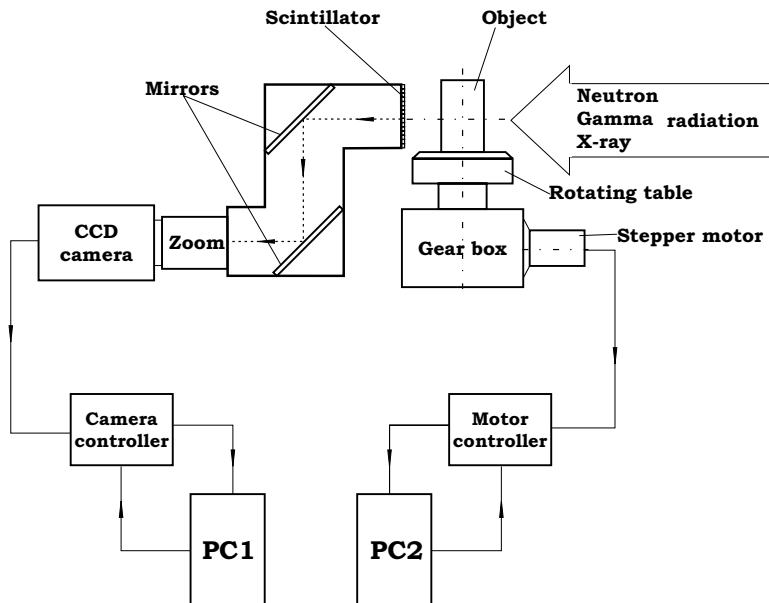


Fig. 6. Imaging apparatus for collecting projections.

appeared as a flickering when playing the projection sequence as a movie. In order to eliminate its effect, we performed intensity correction such that the total intensities of each projection were almost the same constant. It was done by multiplying each projection by a suitable constant.

- A further distorting effect was caused by the noise and white specks in the projections. For the reduction of this effect we applied a thresholded median filter.

Further details about the correction steps and their effects on the reconstruction can be found in [6].

4.4 *Determination of intensity levels*

The next problem was that the exact intensity levels of the image to be reconstructed were unknown. Anyway, in real physical experiments only approximative absorption values can be given, since only average absorption coefficients could be used for polychromatic X-rays. This fact violated one of our basic assumptions, namely the absorption coefficients of the few materials making up the object should have been known exactly. So we had to find a technique to approximate the right absorption values.

In case of the parameter-based method the absorption values could be calculated in virtue of the object geometry. In order to determine the intensity values in the pixel-based case as well, our idea was, first, that we approached the discrete image f of the right values with another image f' having more values. An approximation of the intensity values can be obtained by determining the local maxima in the histogram of f' .

Accordingly, first we did a pixel-based reconstruction using more intensity levels than the number of materials in the object. The set of the enhanced number of intensity levels were produced by the equidistant division of the interval of the possible levels. For example, if the intensity levels are from the interval $[0, 1]$, and 41 intensity levels are picked from that, the enhanced set of levels is $\{0, \frac{1}{40}, \frac{2}{40}, \dots, 1\}$.

In case of the reference cylinder even the background was cut down (see Fig. 7), because it was very noisy, and it degraded the result. Despite of this step the image still remained a 3-level one. A reconstruction result, which was done by using 41 intensity levels from 18 projections, can be seen in Fig. 9. Since the projections were noisy (see Fig. 8 (a) and (b)), and even the method is a statistical one, the intensity levels obtained can be considered only as an approximation of the real ones. However, now we make do with these approximated values. Their more accurate determination is for further researches.

As a following step, it was considered that taking the histogram of this reconstruction result, we can retrieve the approximating intensity levels that can be used for the multi-level DT reconstruction. This retrieval can be performed by the detection of the local maxima in the histogram. In Fig. 10 we introduce the histogram of Fig. 9, where three accumulation points are visible (see pointers in Fig. 10). These intensity levels were used in the multi-level DT reconstruction.

4.5 *Pixel-based reconstruction results*

In view of the intensity values, which are already considered for the DT reconstruction, we performed the pixel-base technique. Its result may be seen in Fig. 11(a). For the sake of comparison we performed ART reconstruction (1000 iterations, relaxation parameter 0.001), which yielded the outcome visible in Fig. 11(b). We chose ART, because if there was a few number of noisy projections, it would give better results than other methods. As seen, some holes appeared in the pixel-based result, which may be due to the noise.

It can also be noticed that in the ART result the background is not black (intensity values vary between 30 and 40), but it should be, since the noisy background was cut down before reconstruction. So, in this case, the pixel-based technique reflects the real absorption values better than ART.

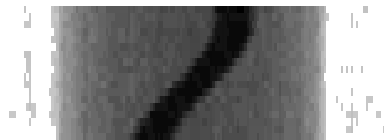


Fig. 7. Sinogram of 18 projections of the cross-section denoted in Fig. 5(b).



Fig. 8. Two projections from the sinogram visible in Fig. 7.

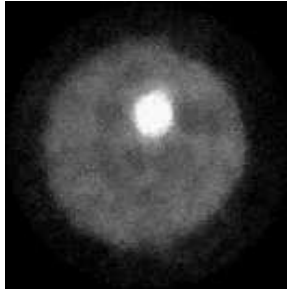


Fig. 9. A reconstruction result (155×155) of the pixel-based method from the sinogram in Fig. 7 using 41 intensity levels.

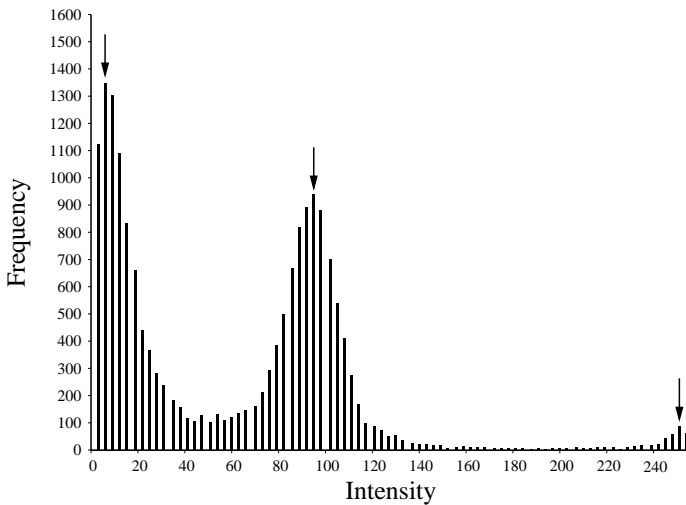


Fig. 10. Histogram of the reconstructed cross-section in Fig. 9. Horizontal axis: Grey-level intensity value. Vertical axis: Frequency of occurrence.

4.6 Parameter-based reconstruction results

In addition to the software experiments mentioned in Subsection 3.2, we had the opportunity to try the parameter-based reconstruction method on physically measured data too. In the experiments we used the reference cylinder introduced in Subsection 4.1. (One of its X-ray projections is shown in Fig. 12(a).) Because of the assumption that every cylindrical hole is filled with the same material, the lower half of the projections had to be discarded (see Fig. 12(b)). The model reconstructed from 4 projections, and the difference of the original and the reconstructed model is seen in Fig. 12(c)–(e) and Fig. 12(f),

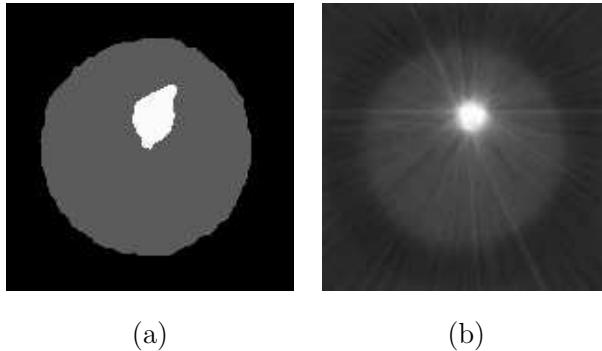


Fig. 11. (a) A pixel-based reconstruction result of the cross-section denoted in Fig. 5(b) using 3 intensity levels. (b) An ART reconstruction yielded by SNARK93 [8].

respectively.

For a more complete description of physical experiments, see [5,6].

5 Discussion and further researches

We implemented two methods. The pixel-based one seems to be promising for the reconstruction of industrial objects (made of a few material) from a small number of projections. It gave good results even in non-ideal, for example, in noisy circumstances using a priori information. Since the absorption coefficients were not known exactly we implemented a technique to retrieve their approximative values.

If the object to be reconstructed is known to be mathematically representable by some parametric functions (e.g., simple geometric primitives like spheres or cylinders), the usage of such a priori information may greatly improve the quality of the reconstructed image, even when fewer projections are available. This is demonstrated by the fact that the parameter-based reconstruction method shows high robustness yet if the projections are degraded by 40% of additive noise.

It is also clear that the parameter-based algorithm is inapplicable if the object cannot be described in a simple geometric way, or when the materials the specimen is made of are not homogeneous. On the other hand, the pixel-based method is unaffected by these circumstances, so it can again be employed successfully. Furthermore, the pixel-based algorithm may benefit from using more intensity levels, whereas the parameter-based one is limited to four absorption values only.

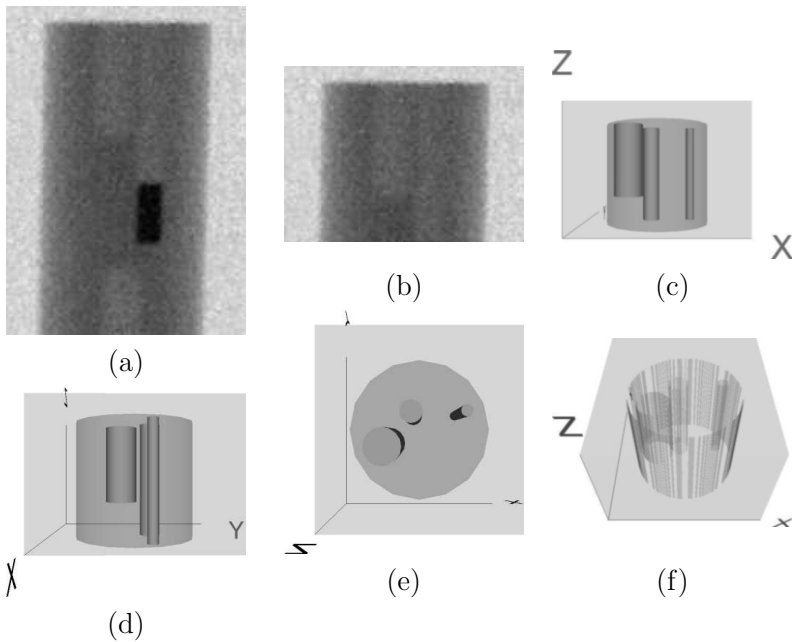


Fig. 12. Projection and reconstruction results of the Plexiglas object given in Fig. 5. (a) One of the original projection images. (b) One of the cropped projection images. (c) 0° view of the reconstructed model. (d) 90° view of the reconstructed model. (e) Top-down view of the reconstructed model. (f) Difference between the reconstructed and original model.

Though the techniques presented here gave promising and acceptable results, we are planning to improve their effectiveness in the future. It would be desirable, for both methods, to speed up the optimization procedure, and to test them on more physically measured projections. The pixel-based technique should be made less sensitive to noise by incorporating a noise model. Finally, some practical extensions of the parameter-based algorithm would be to allow for more than four materials, and using more complex prior knowledge (model) of the object.

References

- [1] Balaskó, M., A. Kuba, A. Nagy, Z. Kiss, L. Rodek, and L. Ruskó, *Neutron-, gamma- and X-ray three-dimensional computer tomography at the Budapest research reactor*, Nuclear Instruments and Methods in Physics Research.A **542** (2005), 302–308.

- [2] Geman, S., and D. Geman, *Stochastic Relaxation, Gibbs distributions, and the Bayesian Restoration of Images*, IEEE Trans. on PAMI **6** (1984), 721–741.
- [3] Herman, G. T., and A. Kuba (Eds.), “Discrete Tomography: Foundations, Algorithms, and Applications”, Birkhäuser, Boston, MA 1999.
- [4] Kirkpatrick, S., C. D. Gelatt, and M. P. Vecchi, *Optimization by simulated annealing*, Science **220** (1983), 671–680.
- [5] Kiss, Z., L. Rodek, and A. Kuba, *Image reconstruction and correction methods in neutron and X-ray tomography*, to be submitted to Acta Cybernetica.
- [6] Kuba, A., L. Rodek, Z. Kiss, L. Ruskó, A. Nagy, and M. Balaskó, *Discrete tomography in neutron radiography*, Nuclear Instruments and Methods in Physics Research.A **542** (2005), 376–382.
- [7] <http://www.inf.u-szeged.hu/~direct/>, Homepage of DIRECT framework, “A toolkit for testing and comparing 2D/3D reconstruction methods of discrete tomography”.
- [8] <http://www.cs.gc.cuny.edu/~gherman/snark2001.html>, Homepage of SNARK93 software system, “A Programming System for 2D Image Reconstruction from Projections”.
- [9] <http://www.web3d.org/x3d/vrml/>, Homepage of VRML97, “Virtual Reality Modeling Language”.